

Can bed load transport drive varying depositional behaviour in river delta environments?

Vegt, H. van der; Storms, J.E.A.; Walstra, D.J.R.; Howes, N.C.

DOI

[10.1016/j.sedgeo.2016.08.009](https://doi.org/10.1016/j.sedgeo.2016.08.009)

Publication date

2016

Document Version

Accepted author manuscript

Published in

Sedimentary Geology

Citation (APA)

Vegt, H. V. D., Storms, J. E. A., Walstra, D. J. R., & Howes, N. C. (2016). Can bed load transport drive varying depositional behaviour in river delta environments? *Sedimentary Geology*, 345, 19 - 32.
<https://doi.org/10.1016/j.sedgeo.2016.08.009>

Important note

To cite this publication, please use the final published version (if applicable).
Please check the document version above.

Copyright

Other than for strictly personal use, it is not permitted to download, forward or distribute the text or part of it, without the consent of the author(s) and/or copyright holder(s), unless the work is under an open content license such as Creative Commons.

Takedown policy

Please contact us and provide details if you believe this document breaches copyrights.
We will remove access to the work immediately and investigate your claim.

Can bed load transport drive varying depositional behaviour in river delta environments?

H. van der Vegt^{* a}, J. E. A. Storms^a, D. J. R. Walstra^{a,b}, N. C. Howes^c

^aDelft University of Technology, Mekelweg 2, 2628 CD Delft, The Netherlands

^bDeltares, Boussinesweg 1, 2629 HV Delft, The Netherlands

^cShell Projects and Technology, 3333 Highway 6 South, Houston, Texas 77082, U.S.A.

Abstract

Understanding the processes and conditions at the time of deposition is key to the development of robust geological models which adequately approximate the heterogeneous delta morphology and stratigraphy they represent. We show how the mechanism of sediment transport (the proportion of the sediment supply transported as bed load vs. suspended load) impacts channel kinematics, delta morphology and stratigraphy, to at least the same extent as the proportion of cohesive sediment supply. This finding is derived from 15 synthetic delta analogues generated by processes-based simulations in Delft3D. The model parameter space varies sediment transport mechanism against proportions of cohesive sediment whilst keeping the total sediment mass input constant. Proximal morphology and kinematics previously associated with sediment cohesivity are also produced by decreasing the proportion of bed load sediment transport. However, distal depositional patterns are different for changes in sediment transport and sediment load cohesivity. Changes in sediment transport mechanisms are also shown to impact clinoform geometry as well as the spatiotemporal scale of autogenic reorganisation through channel avulsions. We

^{*} corresponding author email: h.vandervegt@tudelft.nl

conclude that improving insight into the ratio of bed load to suspended load is crucial to predicting the geometric evolution of a delta.

Keywords

River delta; Sediment transport; Bed load; Suspended load; Cohesive; Process-based modelling

1 Introduction

Understanding deposition in deltaic environments is not only important to predict the effect of anthropogenic changes in these densely populated areas (Syvitski and Saito, 2007), but also forms the basis of geological models of ancient deltaic deposits. The heterogeneous nature of river delta morphology and stratigraphy complicates the development of geological models (Howell et al., 2008). To simplify this process, a number of classification schemes have been developed based on modern deltaic systems. Initially, classification only characterised deltas by the hydrodynamic forces acting on the system (e.g., fluvial input, tidal conditions, wave activity) (Galloway, 1975). Subsequently it was shown that the physical properties of the supplied sediment (e.g., cohesivity, grain size) can be equally important (Orton and Reading, 1993; Hoyal and Sheets, 2009). Past studies have shown that the balance between cohesive and non-cohesive sediments can have significant effects on deltaic morphology (Peakall et al., 2007; Edmonds and Slingerland, 2009; Hoyal and Sheets, 2009; Geleynse et al., 2011).

Comparatively less attention has been given to the effects that sediment transport mechanisms have on deltaic morphology and stratigraphy. Deltaic stratigraphy can be viewed as a record of the sediments preserved by this evolving morphology. Sediment transport ultimately regulates where and how sediment is deposited, based on local

hydrodynamic conditions and sediment properties. Sediment transport to and within a delta environment can be simplified to two mechanisms: bed load and suspended load. In deltaic systems, the majority of sediment supply is typically cohesive and transported in suspension, forming the bulk of the suspended load. A smaller proportion of sediment consists of non-cohesive material (sands) transported partially in suspension and partially through creep and saltation, constituting the bed load.

Field measurements of the suspended load (the cohesive and non-cohesive sediment transported in suspension) is relatively simple and can even be partially automated.

Bed load measurements are more expensive and labour intensive to obtain (Turowski et al., 2010), especially in coastal settings. River deltas are formed at the interface between the fluvial and the coastal domain and are therefore both influenced by fluvial processes as well as marine reworking. Existing work primarily considers fluvial systems with some work having been conducted at coastlines (van Rijn, 2007). In experimental settings of such systems, there are various challenges associated with the scaling of sediment transport (Paola et al., 2009).

Due to the limited data availability, bed load is typically estimated or calculated based on the suspended load measurements (e.g., Syvitski and Saito, 2007, Kleinhans et al., 2012). Turowski et al. (2010) conducted an extensive review of reported values for bed load, but found that often no reference is made to original data. They traced the source of most data back to a data table in a report from the 1950's (Maddock and Borland, 1950) which claimed to "give data on estimates of the unmeasured bed load of streams based on the Bureau of Reclamation experience". Available measurements are mainly for fluvial systems, which Turowski et al. (2010) compiled in their review. It shows that between 1% and 50% of the total sediment load can be transported as bed

load. For ephemeral rivers, however, the percentage can be even higher, up to 100% (Turowski et al., 2010, Karimaee Tabarestani and Zarrati, 2015).

Various factors have been hypothesised to influence the balance between suspended load and bed load transport in fluvial systems. Locally this balance is determined by particle size, weight, shape and hydraulic conditions, while on a larger scale influencing factors may include catchment geology, climate and relief (Laronne and Reid, 1993; Kleinhans and Grasmeijer, 2006; van Rijn, 2007; Turowski et al., 2010; Karimaee Tabarestani and Zarrati, 2015). Turowski et al. (2010) conclude that there is not yet sufficient data available to isolate the effect of different parameters on the partitioning between sediment transported as bed load and suspended load.

Even with this limited data availability, previous studies of river morphologies have identified the proportion of sediment supply transported as bed load as an important control on sediment depositional patterns (Kleinhans, 2010; Turowski et al., 2010; Ashworth and Lewin, 2012). Considering the challenges associated with gathering field data of bed load transport, it is imperative to better understand the implications of these processes on delta morphology and stratigraphy prior to undertaking field studies. In addition, field studies are limited by the availability of appropriate data or field sites and often cannot span the entire parameter space of interest. Comparing different natural systems involves variations in many parameters at the same time. Conducting a modelling study allows the detailed investigation of individual processes and in so doing extend and supplement experimental and field-based studies.

In this study we examine the effect of both sediment transport mechanism and cohesive sediment content on depositional geometries in fluvial dominated deltas. We propose that the mechanism of sediment transport (i.e., what proportion of the

sediment supply is transported as bed load vs. suspended load) impacts depositional behaviour to at least the same extent as sediment properties, such as cohesivity.

In this study we use process-based simulations to assess the effects of sediment transport mechanism compared to sediment composition on deltaic morphology and stratigraphy. As predictions made with process-based models are consistent, and they allow careful control of boundary conditions, the quantitative output can be compared, and specific processes or mechanisms can be isolated. Following this approach we explore three metrics: (1) channel geometry and channel dynamics, (2) locations of sediment deposition, reworking and preservation, and (3) large scale delta geometry. We also discuss the relationships between these quantitative measures. The metrics developed here can be applied to other fluvio-deltaic model ensembles to study the implications of a range of boundary conditions on delta morphology and stratigraphy.

2 Experimental design

We created an ensemble of 15 numerical models using the open source process-based modelling software Delft3D (Lesser et al., 2004). Models were calculated using Delft3D Flow (Version 4168) with parallel processing on a single, Linux operating, 16-core node. For detailed descriptions of the governing equations representing each of the processes as well as the finite difference solution methodology the reader is referred to the Delft3D-Flow documentation which is freely available online. In past studies, Delft3D has been extensively applied to study the effects of hydrodynamic forcing and sediment properties on river delta morphodynamics (e.g., Edmonds and Slingerland, 2009; Geleynse et al., 2010, 2011; 2012; Caldwell and Edmonds, 2014). Our numerical experiments investigate the implications of mechanism of sediment transport on depositional behaviour in a river delta.

2.1 Bathymetry, hydrodynamic forcing and sediment properties

Parameters described in this section were applied to all 15 experiments. The starting bathymetry is similar to that described in previous studies, consisting of a channel delivering water and sediment into a sloped basin already filled with fresh water (Geleynse et al., 2011). One change is that our channel is partially formed by two floodplains sloping toward the basin and channel. This forms a trumpet-shaped channel debouching into the basin, representative of a river mouth towards the end of a rising sea-level cycle. However, sea level was kept constant during the model runs. The initial channel width is 1000 m and with constant discharge of $1500 \text{ m}^3 \text{ s}^{-1}$. This discharge should be considered as a continuous bankfull flood stage. A tide with amplitude of 1 m was added to introduce dynamics into an otherwise very steady system. The effect of flocculation was not considered in this study.

The total sediment supply was estimated based on average suspended load measurements in modern delta systems of a similar scale (Milliman and Farnsworth, 2011). This resulted in a total load concentration of 0.2 kg m^{-3} being applied across the models. The sediment transport calculations do not take migrating bedforms into account, although a Manning roughness coefficient of 0.02 implicitly accounts for the impact of smaller scale bedforms on hydrodynamics.

Calculations span a full hydrodynamic year, but include a morphological scaling factor (MORFAC) of 60 (Ranasinghe et al., 2011). Combining this with continuous bankfull discharge results in deposition equivalent to delta evolution on a millennial timescale. Simulation output was recorded at the end of each of the 366 hydrodynamic days.

2.2 Cohesivity vs. sediment transport

The majority of sediment supplied to deltaic environments consists of a cohesive silt and clay mixture. These sediment types are typically transported as part of the suspended load. Suspended load in Delft3D is calculated by solving a depth-averaged (2DH) advection-diffusion (mass-balance) equation for the suspended sediment (Galappatti, 1983). The remainder of the sediment is non-cohesive (sands and gravels) and is transported partially in suspension, adding to the suspended load, and partially through saltation and creep, constituting the bed load.

Previous simulations of delta formation in Delft3D have used the default Van Rijn (1993) transport formulation (van Rijn, 1993; Edmonds and Slingerland, 2009; Caldwell and Edmonds, 2014) or the Engelund-Hansen transport formulation (Engelund and Hansen, 1967; Geleynse et al., 2011, 2010; Guo et al., 2015) to determine sediment transport of non-cohesive sediment (sands). The Engelund-Hansen formulation reflects total transport. However, its implementation allows for the partitioning of sands into a suspended load and a bed load fraction, for which the transport is calculated separately.

For our simulations, we selected and implemented the Engelund-Hansen transport model after a series of sensitivity studies with the available sediment transport formulas in Delft3D. The total fluvial sediment input of 0.2 kg m^{-3} is made up of four sediment classes, as defined in Figure 1. The properties for the individual sediment classes as well as the total sediment supply concentration are the same in all simulations.

The model parameter space explores the role of sediment transport and sediment composition on delta development. The effect of sediment transport mechanism is explored by varying the relative proportions of bed load versus suspended load

transport. The effect of bulk composition is explored by varying the cohesive versus the non-cohesive sediment fraction. This is done by varying the proportions of the sediments defined in Figure 1. The exact concentrations of each sediment class as well as an estimated D_{50} grain size value of the sediment input is provided in Table 1. Cohesive sediment fractions are defined using a settling velocity rather than a grain size, therefore Stokes' Law is used to convert these values to a grain size value used in the calculation of the overall D_{50} of the sediment supply. As a consequence of varying the balance between cohesive and non-cohesive sediment by means of adjusting the input concentrations of pre-defined sediment classes, the mean grain size value also increases with increasing non-cohesive sediment supply.

The translation of this parameter space into the model input is visualised in Figure 2. To simplify presentation and discussion of the results we have divided the model parameter space in Figure 2 into quadrants. Columns are separated into models with the highest suspended load supply (SL) or models with the highest bed load supply (BL). Rows are divided into models with the highest cohesive sediment supply (CS) or models with the highest non-cohesive sediment supply (NS). These abbreviations will be referred to when comparing depositional trends relating to these differences in cohesivity and sediment transport.

2.3 Analysis and processing

A delta is an evolving landform with morphology and stratigraphy changing over time. To account for the evolution of the depositional behaviour, the analyses were performed per output time interval. Output files contain a record of the bathymetry and the hydrodynamic conditions prevailing at each output time step. This provides insight

into the morphology and stratigraphy as the delta evolves, as well as the processes controlling its evolution.

The first set of analyses pertains to the morphology and kinematics of the channel network. The channels constitute a distributed sediment supply network across the delta top and delta front. In addition to acting as a sediment source, the active channels are also the main erosive features responsible for reworking of sediment.

We defined the active channel network to consist of locations with high sediment transport values together with large flow velocity or erosion. Active channel network locations must have a water depth greater than 0.5 m. Owing to the element size of 50 m x 50 m horizontally, a water depth of less than 0.5 m would imply a width:depth ratio of more than 100. This value falls well outside of the definition of a channel, filtering out sheet flow at the current grid resolution (Gibling, 2006; Hajek and Wolinsky, 2012). Channel depth, a proxy for the erosive properties of the network, has implications for the reworking of underlying sediment. The average channel depth with respect to the elevation of the surrounding delta plain/delta top was also calculated for each model at every time interval.

The channel network does not occupy the same locations over time. As channels prograde into the basin, individual channels can bifurcate, migrate laterally, avulse or become abandoned (Kleinhans, 2010). All of these processes lead to new areas of the delta top becoming incorporated into the active channel network while other areas no longer form part of this network. We calculated the proportion of the active channel network which overlaps with part of the active channel network of the previous output time interval as an indication of channel network mobility. The channel overlap (mobility) has implications for both for the scale of lateral reworking of sediments as

214 well as the distribution of sediment deposition across the delta network (Jerolmack and
215 Mohrig, 2007).

216 Understanding where sediment was deposited and where it was subsequently
217 reworked provides insight into the preserved stratigraphy of the delta. Deposited
218 sediment was divided into four depositional units based on location and depositional
219 processes. These consist of the following categories (Fig. 3):

220 (1) Channel deposits: Consist of accretion deposits as channels migrate or
221 aggrade as well as channel fill following an avulsion. This was defined as any
222 sediment deposited at active channel locations, or at a location that was part of the
223 active channel network until the elevation at that position equals the average elevation
224 of surrounding delta top.

225 (2) Overbank deposits: Consist of sediment deposited on the delta top outside of
226 the active channel network.

227 (3) Lobate deposits: These deposits were defined by rate of deposition, as
228 locations where more than 0.15 m of sediment was deposited in one output time
229 interval. This thickness definition is based on inspection of the results as well as the
230 vertical resolution of the grid. The lobate deposits are supplied by sediment exiting the
231 channel mouths and extend to depths of approximately 15 m to 20 m below sealevel
232 across the model parameter space.

233 (4) Distal deposits: In the case of our analysis, the distal element is a background
234 element consisting of all remaining deposits not yet accounted for within the above
235 elements.

For the purpose of analysis it is necessary to define a clear boundary between lobate and distal deposits, however it is also important to recognise that in natural systems this transition is gradual.

In addition to calculating the depositional units deposited, we are especially interested in the reworking and preservation of these units. The preserved depositional units drive the final geometry of the delta. For example, preserved channel and overbank deposits drive delta top aggradation while preserved lobate deposits drive delta progradation. In order to assess the changes in large scale geometric trends, we calculated the average elevation as a function of distance from the delta apex. For this purpose, radially averaged topographies were constructed as shown in Figure 4. The model results were mapped to polar coordinates with an origin located at the delta apex. This allows each location in the delta bathymetry to be described by the distance from apex and angle from the original coastline. The boundaries on either side of the apex were defined at 20° and 160° respectively to account for the initial trumpet shaped bathymetry. At intervals of active channel elements were not included in the calculation, such that the bathymetry only constitutes the delta top, delta front and prodelta. The elevation was averaged across all angles from 20° to 160° and plotted as a function of distance from apex at intervals of 125 m (Fig. 4B, C). For each model, 366 topographic profiles were constructed, representing the 366 output time intervals (Fig. 4E). For each profile the location of the brink point (separating the delta top and delta front) and delta toe (separating the delta front and pro delta) were identified (Fig. 4D).

3 Results

The ensemble of numerical simulations allows us to study and compare the evolving geometry (morphologic and stratigraphic) and kinematics of the deltas within our parameter space. Figure 5 displays a plan view of the bathymetry at the end of each of the 15 simulations. Bathymetry has been corrected for local water levels. These can be higher proximally due to the backwater effect.

In order to evaluate the depositional behaviour of an evolving landform, we need to compare analyses which account for change in behaviour over time, starting with channel morphology and kinematics. The active channel network acts as a distributed sediment source across the delta top and, as such, drives the location of sediment deposition. Additionally, the active channel network occupies different locations over time, eroding lateral and underlying sediment. Hereby channel kinematics determine the locations at which sediment is reworked. We separate the volume of sediment which is reworked after its initial deposition, obtaining the volume of preserved deposits. Deposited sediment is classified by depositional unit in order to differentiate between the conditions under which the sediment was deposited. Large scale delta geometry is in turn a product of these preserved depositional units.

3.1 Channel morphology and kinematics

In this section we focus on channel properties (morphology and kinematics) which drive sediment deposition and reworking. The channel depth relative to the surrounding delta top elevation was determined for each model in the ensemble. The mean depth (spatially and temporally) was then calculated for each model across all timesteps (Fig. 6). Channels are shallower both with less cohesive sediment supply (Fig. 6, Models 1.1, 2.1, 2.3, 2.4 compared to Models 1.3, 2.4, 3.4, 4.4 respectively)

and less suspended load (Fig. 6, Model 1.1, 1.2, 1.3 compared to Models 4.1, 4.2, 4.3 respectively).

Mean values of channel overlap were calculated (Fig. 6) as a proxy for channel mobility. Channel mobility is greater in BL- and NS-models while channel networks in their corresponding SL- and CS-models tend to occupy the same locations for longer periods of time.

3.2 Sediment reworking and preservation

During the simulation, sediment is deposited in varying quantities across the model domain. At the same time, previously deposited sediment is eroded (reworked) by the evolving channel network. Subtracting the reworked sediment from the total deposited sediment provides the net volume of sediment deposited. This volume of net deposition is reasonably constant for each output time interval. Eroded (reworked) sediment can be re-deposited in one of the following time intervals and ultimately preserved. The cumulative volume of preserved deposits increases over time as the delta progrades and can be calculated as the cumulative net deposition.

The volume of reworked sediment varies significantly between simulations (Fig. 7).

The model where deposited sediment undergoes the most reworking (model 4.4, Fig. 7) shows more than 5 times as much reworking than the model experiencing the least reworking (model 1.1, Fig. 7). In contrast, the volumes of preserved deposits are relatively constant between simulations. The model preserving the largest volume of sediment (model 1.3, Fig. 7) preserves only 1.4 times as much sediment as the model preserving the least (model 4.1, Fig. 7).

More sediment deposited in BL-models undergo reworking than in SL-models. This is illustrated by the larger blue area in models 1.3, 2.4, 3.4, and 4.4 (Fig. 7) compared to

models 1.1, 2.1, 3.1 and 4.1 (Fig. 7) respectively. To a lesser extent, slightly more sediment deposited in NS-models undergoes reworking compared to those deposited in CS-models. This is illustrated by the larger blue area in models 4.1, 4.2, 4.3 and 4.4 (Fig. 7) compared to models 1.1, 1.2, 1.3 and 2.4 (Fig. 7) respectively. Therefore, both more bed load transport or more non-cohesive sediment leads to a greater volume of sediment reworking. As the delta evolves, the volume of reworked sediment per output time interval increases and the differences between the models become even more pronounced. Therefore, both an increase in bed load transport and decrease in sediment cohesion can drive divergent behaviour delta top reworking.

The total deposited sediment was classified into four depositional units: channel deposits, overbank deposits, lobate deposits and distal deposits. This classification was also extended to the reworked and preserved deposits. Sediment reworking occurred mainly in channel and overbank deposits, which constitute the delta top, and to a smaller extent in the lobate deposits which are found mainly in the delta front (Fig. 8). Only in shallower, proximal regions, where a thinner layer of channel, overbank and lobate sediments were deposited (as a result of the sloped basin), did sediment erosion reach older distal deposits or initial substrate (e.g., Fig. 3). Sediment eroded from the substrate contributed less than 0.2% of the total sediment supplied to the systems and was not included in the analyses.

SL-CS models (model 1.1, 1.2, 2.1, 2.2) show smaller volumes of delta top reworking compared to BL-NS models (models 3.3, 3.4, 4.3, 4.4). SL-CS models also exhibit larger proportion of lobate and distal deposit reworking. As the delta top grows over time, a larger volume of channel and overbank deposits undergo reworking within each time interval (Fig. 8). This divergent behaviour is strongest in BL-NS models (models 3.3, 3.4, 4.3, 4.4) while it is barely discernible in SL-CS models (model 1.1,

1.2, 2.1, 2.2). Lobate and distal deposits undergo a more uniform volume of reworking over time.

The proportion of the preserved depositional units reaches a reasonably steady state for each delta (Fig. 9). The proportions of different depositional units being preserved, although differing between models, is not a divergent characteristic of delta evolution. Figure 9 shows that across this dataset, the channel deposits contributed 18% to 27% of the total deposited volume, lobate deposits contributed 21% to 34%, overbank deposits contributed 6% to 8% and distal deposits contributed 38% to 49%.

The proportion of channel deposits is larger in NS-models compared to their corresponding CS-models. This can be seen from models 4.1, 4.2, 4.3 and 4.4 which have a 2% to 11% larger proportion of channel deposits than models 1.1, 1.2, 1.3 and 2.4 respectively (Fig. 9). A larger proportion of channel deposits with more bed load is less pronounced and there are outliers to this trend (e.g., models 4.1 and 2.1 in Fig. 9 should strictly have less channel deposits for this trend to hold in all rows).

The analyses presented thus far is closely related to the evolution of the channel network and SL- to BL- models (left to right in Figs. 5 - 8) exhibited similar trends behaviour to CS- to NS-models (top to bottom in Figs. 5 t- 8). This relationship reverses for the preservation of lobate deposit, where SL- to BL-models trends (left to right in Figs. 4 - 8) corresponds to NS to CS-models trends respectively (bottom to top in Figs. 4 - 8). The volume of lobate deposits is smaller in SL-models than in BL-models. This can be seen in Fig. 9 where models 1.3, 2.4, 3.4, and 4.4 preserve between 3% and 9% more lobate deposits compared to models 1.1, 2.1, 3.1 and 4.1, respectively. However, larger proportions of lobate deposits are preserved in CS-models compared to NS-models. This can be seen in Fig. 9 where models 1.1, 1.2, 1.3

and 2.4 preserve between 1% to 9% more lobate deposits to models 4.1, 4.2, 4.3 and 4.4, respectively.

Overbank deposits account for only a small proportion (6-8%) of the preserved deposits and is the highest in model 4.1 (Fig. 9). Preserved overbank deposition is higher in systems with non-cohesive sediment supply and systems which favours suspended load transport.

Conversely to channel deposits, preserved proportion of distal deposits is larger when suspended load transport is greater. SL-models 1.1, 2.1, 3.1 and 4.1 have a 5% to 9% larger proportion of distal deposits compared to models 1.3, 2.4, 3.4 and 4.4, respectively (Fig. 9). In the distal deposits the correlation with cohesivity is less continuous with outliers to the trend (e.g., model 1.3 should strictly have a larger proportion of distal deposit and model 2.1 less for the trend to hold in all columns).

3.3 Evolution of delta geometry

The averaged topographic profile of each delta, which represents the overall bathymetry at every output time interval by a single line (Fig. 4), evolves as the delta progrades (Fig. 10).

The horizontal brink point displacement is a proxy for delta top progradation. The delta top progrades further into the basin in BL-models than in SL models. This can be seen from the horizontal brink point displacement (Table 2) which is 40% to 80% more in models 2.4, 3.4 and 4.4 compared to models 2.1, 3.1 and 4.1, respectively. No trend on delta top progradation is detected between CS- and NS models.

The horizontal delta toe displacement is a proxy for delta front progradation. The delta front progrades further into the basin in CS-models than in NS-models. This can be

seen from the horizontal delta toe displacement (Table 2) which is which can be up to three times as much in CS models compared to its respective NS-model (model 1.2 compared to model 4.2). The same trend is present between SL-models, where the delta toe can prograde up to twice as far into the basin compared to BL-models (model 2.1, SL-model, compared to model 2.4, corresponding BL-model).

Proximal vertical displacement was calculated at 2 km distance from the delta apex and serves as a proxy for the level of proximal delta top aggradation. A distance of 2 km was chosen as more proximal areas contain too many of the active channel network elements (excluded from the calculation) compared to delta top elements and therefore does not give a representative estimate of the delta top elevation when averaged. The delta top aggrades more in BL-models than in SL-models. Table 2 shows that BL models (e.g., models 2.4, 3.4, 4.4) can undergo 40% to 60% more proximal vertical aggradation than their respective SL-models (models 2.1, 3.1, 4.1). The same trend is present for NS-models compared to CS-models, but here the aggradation is only 10% to 30% model in NS-models (e.g., Model 4.1, 4.2 and 4.3) compared to their respective CS models (models 1.1, 1.2, and 1.3).

The delta top slope for all models are approximately horizontal, varying between 0.04% and 0.05% between models, corresponding to 0.02 degrees to 0.03 degrees. The delta front slopes are steeper than the delta top slopes, starting at approximately 0.3% initially, corresponding to 0.2 degrees (Fig. 11). The delta front slopes steepen up to 0.8% (Fig. 11, model 2.4) at the end of the simulation, corresponding to 0.5 degrees. The delta front slope steepens faster in BL-models (Fig. 11, dashed lines, models 1.3, 2.4, 3.4 and 4.4) compared to their corresponding SL-models (Fig. 11, solid lines, models 1.1, 2.1, 3.1 and 4.1)

In the averaged topographic profiles of some models, degradation stacking (Neal and Abreu, 2009) is observed (Fig 10). This is particularly visible in SL-models (models 1.1, 2.1, 3.1 and 4.1) and CS-models (models 1.1, 1.2 and 1.3). This is however an artefact of a longer timescale between channel network avulsions leading to a more rugose shoreline in these models (Model 1.1 compared to Model 1.3, Fig. 5). This is explained in Figure 12, which shows the central lobe in model 1.1 prograding further from the delta apex than the shore-proximal lobes (Fig. 12A interval 50, 12B interval 75, 12C interval 100), which produces an apparent degradational averaged topographical profile. Once an avulsion occurs which starts to fill up this shore-proximal bay (Fig. 12D, output time interval 125), the averaged topographic profile begins to even out to a progradational stacking pattern again. Therefore the apparent degradation stacking patterns visible in the averaged topographic profiles are representative of larger timescales for the onset of autogenic events in the models, in particular lobe switching activity. Figure 10 therefore shows that SL- models and CS-models have a larger timescale for the onset of autogenic events than their corresponding BL-models and NS-models.

4 Discussion

We developed and employed a set of general metrics to compare deposits from an ensemble of synthetic deltas. These metrics fall into three categories:

1. Channel morphology and kinematics,
2. Sediment reworking and preservation,
3. Large scale delta geometry.

These depositional responses are interdependent, as the evolving system strives to reach optimal hydraulic efficiency.

In the prograding systems of the model ensemble, the driving force behind delta evolution is fluvial input, supplied to the delta through the distributary channel network. The evolution of the channel network is therefore key in describing the depositional behaviour of the system. However more distal depositional behaviour, such as the delta front slope and the volume of lobate deposits, shows less correlation to the difference in the channel network morphology and kinematics, and transport and settling behaviour of the sediment becomes more important.

We have identified gradual differences in the geometric depositional patterns from bed load (BL) systems to suspended load (SL) systems and we discuss the end-members of these systems separately. BL systems exhibit many, but not all, of the same characteristics as non-cohesive (NS) systems, and the differences and similarities are discussed separately.

4.1 *Suspended load systems*

The degree of channel network overlap from one output time interval to the next is a proxy for channel mobility, reflecting both avulsion and lateral migration of channels.

Suspended load systems (SL-models) have low channel mobility. The suspended sediment (cohesive plus suspended non-cohesive sediment) in the SL-models can readily bypass the channel network, limiting vertical aggradation within the channels.

Channels therefore erode deeper into the underlying delta deposits than in BL-models.

Active channels occupy the same location for a longer time, producing localised lobate deposits over and through which the channel progrades into the basin. This leads to a rugose delta brink contour (Fig. 3). After an avulsion occurs in these systems, it leaves

a deep abandoned channel feature in the delta top which is initially unfilled but which no longer forms part of the active channel network. Together with the rugose delta brink development, this contributes to a larger variability in delta top geometry in SL-models.

The low channel mobility not only affects delta top geometry, but also implies that channels rework a limited area of the delta top. Delta top deposits (channel and overbank) override the older lobate deposits and even older distal deposits. Since SL-models produced deeper channels, channel erosion can reach down to underlying lobate and distal deposits more readily. The extent to which the underlying deposits are reworked also depends on the thickness of the delta top deposits. The low mobility of the channel network produces elongated, prograding channels which transport sediment deeper into the basin. More sediment is transported to the delta front and prodelta rather than being distributed on the delta top. Therefore the delta top does not aggrade, but instead the delta front progrades further into the basin. The reworking of these vertically stacked architectural elements, over a limited horizontal area, could produce a heterogeneous distribution of delta facies, disconnected by the deep channel features.

These deep channel features and heterogeneous facies distributions correspond to what has previously been described as a topset-dominated delta (Edmonds et al., 2001). However all the models analysed here fall into the category of foreset-dominated deltas based on their channel depth and foreset-thickness.

As suspended sediment transport increases (Fig. 9, right to left), there is a gradual change in sediment dispersal from favouring channel and proximal lobate deposits to increasingly distal deposition. The delta front in SL-models consists of a thin,

elongated sediment bed which gradually blends into the prodelta distally. Once deposited, proximal lobate deposits at the delta brink are soon partially reworked by the prograding, low mobility channel from which it was initially deposited. Together with the deeper channels in SL-models which reach down to rework older lobate deposits, the reworking of lobate deposit at the channel mouth causes a smaller proportion of the lobate deposits to be preserved compared to BL-models. The reworked lobate deposits are then redeposited further into the basin or as overbank deposits. This causes the delta toe (and by proxy the delta front) to prograde further into the basin in SL-models. Less delta top aggradation and progradation and more delta front progradation in SL-models leads to elongated clinoforms which steepen at a slower rate than in the corresponding BL-models.

In addition, low channel mobility lead to a larger temporospatial scale of autogenic lobe switching events, which can be seen from the apparent degradational clinoforms in the averaged topographical profiles (e.g., Model 1.1 or 2.1, Fig. 10) as explained in Fig. 12.

4.2 Bed load systems

BL-models exhibit highly mobile channel networks with frequent avulsions. The bed load transport constrains sediment to the channel network during both transport and deposition. This causes vertical aggradation, increasing the rate of avulsion.

Overloading of bed sediment has previously also been linked to vertical channel aggradation followed by avulsion (e.g., Kleinhans et al., 2012).

This means more bed load transport leads to shallower channels features, which contribute to less geometric variability in delta top geometry than the deep channels of the SL-models. In addition, the highly mobile channel network distributes sediment

smoothly across the entire delta front and delta top creating a smooth delta brink contour (Fig. 5, models 1.3, 2.4, 3.4 and 4.4 compared to models 1.1, 2.1, 3.1 and 4.1, respectively). Repeated reworking by the channel network in the BL-models further smooths delta top geometry.

Together with the smooth, reworked delta top, the vertical aggradation in the channel network causes the entire delta top to aggrade over time. This is most pronounced at proximal locations, which have undergone aggradation and reworking for a longer period than the distal locations. The rise in proximal floodplain elevation in the simulations leads to a rise in water level. This creates additional accommodation in inter-distributary/bay areas, which future channel avulsions may occupy. It is not possible to isolate whether the aggradation drives the channel dynamics or whether the channel dynamics drive the aggradation. Most likely the channel dynamics and delta top aggradation create a constructive feedback effect in high bed load systems.

The channel mobility in systems characterised by bed load transport causes a large area of the delta top to be reworked by the channels. The shallow channels do not frequently erode into the underlying lobate and or distal deposits. Therefore reworking is mainly constrained to the upper layers of channel and overbank deposits which constitute the delta top. This leads to a more uniformly stacked stratigraphy of distal deposits, overridden by lobate deposits, which in turn is overridden by a mixture of channel and overbank deposits which at the delta top. This homogeneous geometry and distribution of depositional units is consistent with that described for foreset-dominated deltas (Edmonds et al., 2011).

Bed load not deposited in active channel network is transported towards the channel mouth where it is deposited as lobate deposits. When the downstream distance along

the channel becomes too large for sediment to be transported to the channel mouth, channels aggrade vertically, eventually leading to avulsion (Kleinhans et al., 2012). This increases the proportion of sediment deposited close to the channel network (channel and proximal lobate deposit) at the expense of overbank and distal deposits. The shallower, aggradational channels are also less likely to rework lobate deposits at the channel mouth or reach down to it as the channels traverse the delta top. Therefore BL-models preserve a larger quantity of especially proximal deposits. This preferential proximal deposition means that more bed load transport in a deltaic system causes more delta top aggradation and progradation and less delta front progradation into the basin. This also increases the rate at which the delta front slope steepens as the delta progrades into the basin. The clinoforms in BL-deltas are smooth (Fig. 10) compared to those in SL-models, indicating a shorter temporospatial scale of autogenic lobe switching events than in SL-models.

4.3 The role of sediment transport compared to cohesive sediment supply on deltaic deposition

Based on the analyses presented, kinematics, channel morphology and channel deposits undergo a similar shift in behaviour if the proportion of suspended load is greater (SL-models) or if the proportion cohesive sediment is greater (CS-models). In both these cases channels will be deeper, channel kinematics will be less, leading to less delta top reworking, a more heterogeneous geometric distribution of depositional units, and a more rugose shoreline. Low channel mobility such as that seen in SL-models, has also previously been associated with cohesive sediment (Edmonds and Slingerland, 2009; Hoyal and Sheets, 2009; Edmonds et al., 2011; Geleynse et al., 2011).

In the case of suspended load systems, however, the preserved proportion of channel deposits is only weakly correlated with decrease in channel kinematics and the proportion of lobate deposit is also less with lower channel kinematics. In the case of cohesive systems, however, this correlation between channel kinematics and channel deposits is strong, but an increase in lobate deposits is observed rather than the decrease seen in suspended load systems.

We also observe no trend in delta front progradation between models where only the cohesivity is varied, although there is a very strong change in delta front progradation with increasing cohesivity (Fig. 10, compare models in each column). On the other hand, there is a definite increase in delta top progradation with increasing bed load transport, but a smaller correlation of sediment transport with delta toe progradation (Fig. 10, compare the models in each row).

In order to understand the above similarities and differences, we need to understand the difference between varying the proportion of cohesive sediment supply compared to varying the proportion of suspended load transport in the simulations. The average sediment supply D_{50} is lower in cohesive compared to non-cohesive simulations (Table 1), while the balance between suspended load and bed load only changes the transport mechanism and not the D_{50} of the sediment supply. Smaller grain sizes mean lower settling velocities and therefore more sediment bypasses the delta top, depositing as lobate and distal deposits in the delta front and prodelta positions instead. Similar responses to grain size have been recorded in the literature (Caldwell and Edmonds, 2014).

Our findings indicate that while both suspended load and cohesive sediment can change the distributary network morphodynamics in the same way, they influence

deposition more distal from the network in distinctly different ways. Sediment supply composition is shown to change the progradation of the delta front while not exhibiting a clear trend in delta top progradation or delta front slope. Sediment transport mechanism was shown to strongly influence the rate at which the delta front steepens and the delta top progrades, while more weakly influencing the progradation of the delta front.

4.4 From synthetic analogues to natural systems

The model results are presented as synthetic analogues to analyse the effects of sediment transport on the general depositional behaviour in natural systems. This requires consideration of the differences between the synthetic analogues and natural systems.

We investigate variations in the mechanism of sediment transport (suspended vs. bed load) independently from variation in sediment cohesivity. However, in natural deltaic systems these two aspects are related. Bed load transport in deltaic systems is still poorly understood and it has been suggested that it should not be calculated as a function of suspended load but as a separate entity (Kazemi et al., 2012).

One process which has been linked to the proportion of bed load transport in fluvial systems is flooding (Karimaei Tabarestani and Zarrati, 2015). Our simulations impose constant discharge, which limits the amount of channel over-spilling, and may underestimate overbank deposition. Due to the link between floods and higher proportions of bed load transport, an underestimation of overbank deposits is likely more relevant for systems with high bed load transport (BL-models). At the same time, we do not model low stage discharge, which would be dominated mainly by

suspended load. During these low discharges, overbank deposits are unlikely to be generated and the models could therefore also overestimate overbank deposition.

In natural systems the relationship between suspended load and bed load is not constant (Laronne and Reid, 1993; Chatanantavet et al., 2012; Karimae Tabarestani and Zarrati, 2015). During peak flow events, bed load transport may constitute a much higher proportion of the total load (Turowski et al., 2010). Lamb et al. (2012) suggest that flooding can increase erosion in the backwater region. We assume a constant flooding stage, which lacks the base flow discharge. Future work could investigate the effect that varying flow between flooding and base discharge has on the balance between aggradation and erosion of the floodplain and subaqueous delta top.

We identified different patterns of aggradation, progradation and retrogradation in the averaged topographic profiles (Fig. 10) which match with some of the patterns described in Neal and Abreu (2009). However, our simulations represent at most deposition on an intraparasequence scale. By the end of the simulations the delta front slope reaches between 0.3° and 0.5° , which is considered shallow for a delta front slope (Korus and Fielding, 2015). However the delta front slopes are still increasing, and therefore for longer simulations or a steeper initial basin slope it is expected that a steeper delta front slope would be reached.

All heterogeneities in the geometry and stratigraphy of the simulation are driven by autogenic self-organisation of the depositional system. The delta front slopes of the different models steepen at different rates, and it is therefore postulated that the difference in delta front slope between the different models will diverge further for longer simulations, at least up to the autobreak point (Muto et al., 2007). The constant sediment supply and zero change in accommodation corresponds to sealevel stillstand

as described by Muto et al. (2007). However our simulations do not prograde long enough to reach an autobreak. The lower rate of steepening in the suspended load systems also means that sediment is spread over a larger area and therefore it may reach an autobreak point earlier than a corresponding system with large proportions of bed load transport.

The set of metrics presented here allow objective comparison of the evolution of deltaic deposits in four dimensions. When comparing model results, we are able to vary a single variable and study its influence in great detail between consistent experiments. Databases comparing modern deltaic systems investigate deposition in geomorphological sub-environments and considers predictive controls on their morphodynamics (Syvitski and Saito, 2007; Korus and Fielding, 2015). These natural systems respond to the interaction of a wide range of boundary conditions (e.g., climate, accommodation space, sediment transport, discharge, marine processes, river power, wave energy, tidal energy). In addition deposition responds to the number, magnitude and sequence of events occurring during deposition (e.g., floods, tectonism, sealevel changes) (Syvitski and Saito, 2007). Due to this large variety of influencing factors, a comparison of natural systems does not allow the definitive association of depositional patterns to differences in a single boundary condition. The strength of a process-based modelling approach, as presented here, is that it allows the analysis of depositional responses to changes in a single variable.

5 Conclusions

The mechanism of sediment transport was shown to have at least as big an impact on delta kinematics, morphology and stratigraphy as sediment cohesivity. When sediment cohesivity remains constant, morphology previously associated with sediment

639 cohesivity could also be produced by increasing the proportion of suspended load
640 sediment transport. Differences in channel kinematics can be due to the mechanism of
641 sediment transport or the supply composition. We found channel kinematics to be a
642 key factor in predicting the evolution of proximal depositional patterns in deltas, but
643 that distal depositional trends respond differently to changes in sediment supply and
644 sediment transport mechanisms.

645 The similarities between the depositional responses of bed load systems and non-
646 cohesive sediment supply highlight how a deltaic sediment body can originate from a
647 non-unique sequence of depositional controls and events. During the dynamic
648 evolution of a delta's stratigraphy and morphology numerous processes and controls
649 interact. While calculated values for bed load transport for modern systems have been
650 reported in databases of modern deltaic systems (Syvitski and Saito, 2007; Korus and
651 Fielding, 2015), our models highlight the influence of these sediment transport
652 mechanisms on long term delta evolution. In addition to sediment budget and
653 sediment supply composition, the effect of the mechanism of sediment transport, and
654 its geometric implication on the preserved stratigraphy, should be considered when
655 creating geological models of deltaic deposits.

656 Previous authors stated that models prograding during a sealevel stillstand (as in our
657 simulations) do not have a characteristic temporospatial scale for autogenic events
658 due an ever-decreasing rate of progradation (Muto et al., 2007). However in our
659 simulations, bed load systems and non-cohesive systems undergo more frequent and
660 smaller autogenic reorganisations than suspended load systems and cohesive
661 systems. If it is true that the stratigraphic products of large scale autogenic processes
662 can easily be misinterpreted as those of allogenic processes (Muto et al., 2007), then

our work suggests that this risk is higher in systems which high suspended load or higher levels of cohesive sediment supply.

We conclude that a better insight into the ratio of bed- to suspended load is crucial to predicting morphologic and stratigraphic aspects of a delta.

Acknowledgements

This work received financial support from Deltares and Shell. The simulations were carried out on the Dutch national e-infrastructure with the support of SURF Foundation (NWO project MP-293-14). We would like to thank Liang Li for many useful discussions during the development of this work, Bert Jagers for his help answering questions relating to Delft3D and Matthew Wolinsky for help during the development of the analysis. We would also like to thank the two anonymous reviewers for their feedback, which helped to improve the text.

References

- Ashworth, P.J., Lewin, J., 2012. How do big rivers come to be different? *Earth-Science Reviews* 114, 84–107.
- Caldwell, R.L., Edmonds, D.A., 2014. The effects of sediment properties on deltaic processes and morphologies: A numerical modeling study. *Journal of Geophysical Research: Earth Surface*, 119, 961–982.
- Edmonds, D.A., Slingerland, R.L., 2009. Significant effect of sediment cohesion on delta morphology. *Nature Geoscience* 3, 105–109.
- Edmonds, D.A., Shaw J.B., Mohrig, D., 2011. Topset-dominated deltas: A new models for river delta stratigraphy. *Geology* 29, 1175-1178.

685 Engelund, F., Hansen, E., 1967. A monograph on Sediment Transport in Alluvial
 686 Streams. Teknisk Forlag, Skelbregade 4, Copenhagen V, Denmark, 59pp.

687 Galappatti, R., 1983. A depth integrated model for suspended transport. Delft
 688 University of Technology, Delft, The Netherlands, 111pp.

689 Galloway, W.D., 1975. Process Framework for describing the morphologic and
 690 stratigraphic evolution of deltaic depositional systems. In: Deltas: Models for
 691 Exploration. Houston Geological Society, Houston, USA, pp. 86–98.

692 Geleynse, N., Storms, J.E.A., Stive, M.J.F., Jagers, H.R.A., Walstra, D.J.R., 2010.
 693 Modeling of a mixed-load fluvio-deltaic system. *Geophysical Research Letters* 37,
 694 doi:10.1029/2009GL042000

695 Geleynse, N., Storms, J.E.A., Walstra, D.J.R., Jagers, H.R.A., Wang, Z.B., Stive,
 696 M.J.F., 2011. Controls on river delta formation; insights from numerical modelling.
 697 *Earth and Planetary Science Letters* 302, 217–226.

698 Geleynse, N., Voller, V.R., Paola, C., Ganti, V., 2012. Characterization of river delta
 699 shorelines. *Geophysical Research Letters* 39, doi:10.1029/2012GL052845

700 Gibling, M.R., 2006. Width and Thickness of Fluvial Channel Bodies and Valley Fills in
 701 the Geological Record: A Literature Compilation and Classification. *Journal of*
 702 *Sediment Research* 76, 731–770.

703 Guo, L., van der Wegen, M., Roelvink, D.J.A.A., Wang, Z.B., He, Q., 2015. Long-term,
 704 process-based morphodynamic modeling of a fluvio-deltaic system, part I: The role of
 705 river discharge. *Continental Shelf Research* 109, 95–111.

706 Hajek, E.A., Wolinsky, M.A., 2012. Simplified process modeling of river avulsion and
 707 alluvial architecture: Connecting models and field data. *Sedimentary Geology* 257-260,
 708 1–30.

709 Howell, J. A., Skorstad, A., MacDonald, A., Fordham, A., Flint, S., Fjellvoll, B.,
 710 Manzocchi, T., 2008. Sedimentological parameterization of shallow-marine reservoirs.
 711 *Petroleum Geoscience* 14, 17-35.

712 Hoyal, D.C.J.D., Sheets, B.A., 2009. Morphodynamic evolution of experimental
 713 cohesive deltas. *Journal of Geophysical Research: Earth Surface* 114(F2),
 714 doi:10.1029/2007JF000882

715 Jerolmack, D.J., Mohrig, D., 2007. Conditions for branching in depositional rivers.
 716 *Geology* 35, 463–466.

717 Karimaei Tabarestani, M.K., Zarrati, A.R., 2015. Sediment transport during flood
 718 event: a review. *Journal of Environmental Science and Technology* 12, 775–788.

719 Korus, J.T., Fielding, C.R., 2015. Asymmetry in Holocene river deltas: Patterns,
 720 controls, and stratigraphic effects. *Earth-Science Reviews* 150, 219-242.

721 Kleinhans, M.G., 2010. Sorting out river channel patterns. *Progress in Physical*
 722 *Geography* 34, 287–326.

723 Kleinhans, M.G., de Haas, T., Lavooi, E., Makaske, B., 2012. Evaluating competing
 724 hypotheses for the origin and dynamics of river anastomosis. *Earth Surface Processes*
 725 *and Landforms* 37, 1337–1351.

726 Kleinhans, M.G., Grasmeijer, B.T., 2006. Bed load transport on the shoreface by
 727 currents and waves. *Coastal Engineering* 53, 983–996.

728 Laronne, J.B., Reid, I., 1993. Very high rates of bedload sediment transport by
729 ephemeral desert rivers. *Nature* 366, 148–150.

730 Lesser, G.R., Roelvink, D.J.A., van Kester, J.A.T.M., Stelling, G.S., 2004.
731 Development and validation of a three-dimensional morphological model. *Coastal*
732 *Engineering* 51, 883–915.

733 Maddock, T., Borland, W.M., 1950. Sedimentation Studies for the Planning of
734 Reservoirs by the Bureau of Reclamation. Technical Report, United States
735 Department of the Interior, Bureau of Reclamation, Branch of Project Planning.

736 Milliman, J.D., Farnsworth, K.L., 2011. River Discharge to the Coastal Ocean: A
737 Global Synthesis. Cambridge University Press, Cambridge, 382pp.

738 Muto, T., Steel, R.J., Swenson, J.B., 2007. Autostratigraphy: A framework norm for
739 genetic stratigraphy. *Journal of Sedimentary Research* 77, 2-12.

740 Neal, J., Abreu, V., 2009. Sequence stratigraphy hierarchy and the accommodation
741 succession method. *Geology* 37, 779-782.

742 Orton, G.J., Reading, H.G., 1993. Variability of deltaic processes in terms of sediment
743 supply , with particular emphasis on grain size. *Sedimentology* 40 475–512.

744 Paola, C., Straub, K., Mohrig, D., Reinhardt, L., 2009. The “unreasonable
745 effectiveness” of stratigraphic and geomorphic experiments. *Earth-Science Reviews*
746 97, 1–43.

747 Peakall, J., Ashworth, P.J., Best, J.L., 2007. Meander-Bend Evolution, Alluvial
748 Architecture, and the Role of Cohesion in Sinuous River Channels: A Flume Study.
749 *Journal of Sediment Research* 77, 197–212.

750 Ranasinghe, R., Swinkels, C., Luijendijk, A., Roelvink, D.J.A., Bosboom, J., Stive,
 751 M.J.F., Walstra, D.J.R., 2011. Morphodynamic upscaling with the MORFAC approach:
 752 Dependencies and sensitivities. *Coastal Engineering* 58, 806–811.

753 Syvitski, J. P. M., Saito, Y., 2007. Morphodynamics of deltas under the influence of
 754 humans. *Global and Planetary Change* 57, 261-282.

755 Turowski, J.M., Rickenmann, D., Dadson, S.J., 2010. The partitioning of the total
 756 sediment load of a river into suspended load and bedload: A review of empirical data.
 757 *Sedimentology* 57, 1126–1146.

758 van Rijn, L.C., 2007. Unified View of Sediment Transport by Currents and Waves. I:
 759 Initiation of Motion, Bed Roughness, and Bed-Load Transport. *Journal of Hydraulic*
 760 *Engineering* 133, 649-667

761 van Rijn, L.C., 1993. Principles of sediment transport in rivers, estuaries and coastal
 762 seas. Aqua publications, Amsterdam, The Netherlands.

763 **Figure captions**

764 Fig. 1. Bathymetry and boundary conditions for all models in the simulation ensemble
 765 with sample simulation output for model 2.3 (top right). The input boundary conditions
 766 include discharge and sediment input at the fluvial boundary and a semi-diurnal tide at
 767 the distal basin boundary.

768 Fig. 2. Variation in boundary conditions for the models used in this study. Sediment
 769 transported as bed load (orange) increases from left to right at the expense of
 770 suspended load (blue). The proportion of non-cohesive sediment supply (yellow)
 771 increased downwards at the expense of cohesive sediment (brown). Total load

concentration is constant at 0.2 kg/m^3 across all models. Model 1.4 does not exist as it is not possible to define 35% bed load from only 30% non-cohesive sediment.

Fig. 3. Distribution of preserved depositional units at the end of simulation for Model 2.3

Fig. 4. Illustration of the construction of the averaged topographic profiles. (A) The original and example output bathymetry of a single output time interval in one model. (B) Elevation of the non-channel bathymetry points averaged radially around the delta apex, plotted as a function of distance from apex to create a single averaged topographic profile (C). (D) For each profile a delta toe and delta brink point is identified which defined the geometric regions delta top, delta front and prodelta. (E) The process is repeated at each time interval and plotted for every 25th time interval, with blue being the oldest profile and orange the youngest.

Fig. 5. Bathymetry of model ensemble at the end of the simulation. Elevation values were normalised for localised differences in water level.

Fig. 6. Channel network area with percentage of the active channel network area overlapping with that of the previous time interval indicated in yellow. The mean overlap (%) is calculated and illustrated as an orange line. Mean channel depth (m) with respect to the adjacent delta top/flood plain is displayed in the bottom right corner of each graph.

Fig. 7. Total volume of sediment deposited over time for all 15 models (blue plus orange area), as it evolves over time. The blue area represents the volume which is eroded (reworked) in each time interval and the orange area the net volume of sediment deposited/preserved per time interval as the delta progrades.

795 Fig. 8. Composition of the reworked sediment by depositional units.

796 Fig. 9. Evolution of total preserved deposit throughout the simulation, by depositional
797 units. The average proportions of channel and delta front deposits at the end of the
798 simulation are also shown.

799 Fig. 10. Evolution of averaged topographic profile of each model over time. Fourteen
800 of the 366 topographic profiles spanning the evolution of each simulated delta are
801 displayed. Blue shows the oldest profile and orange the youngest.

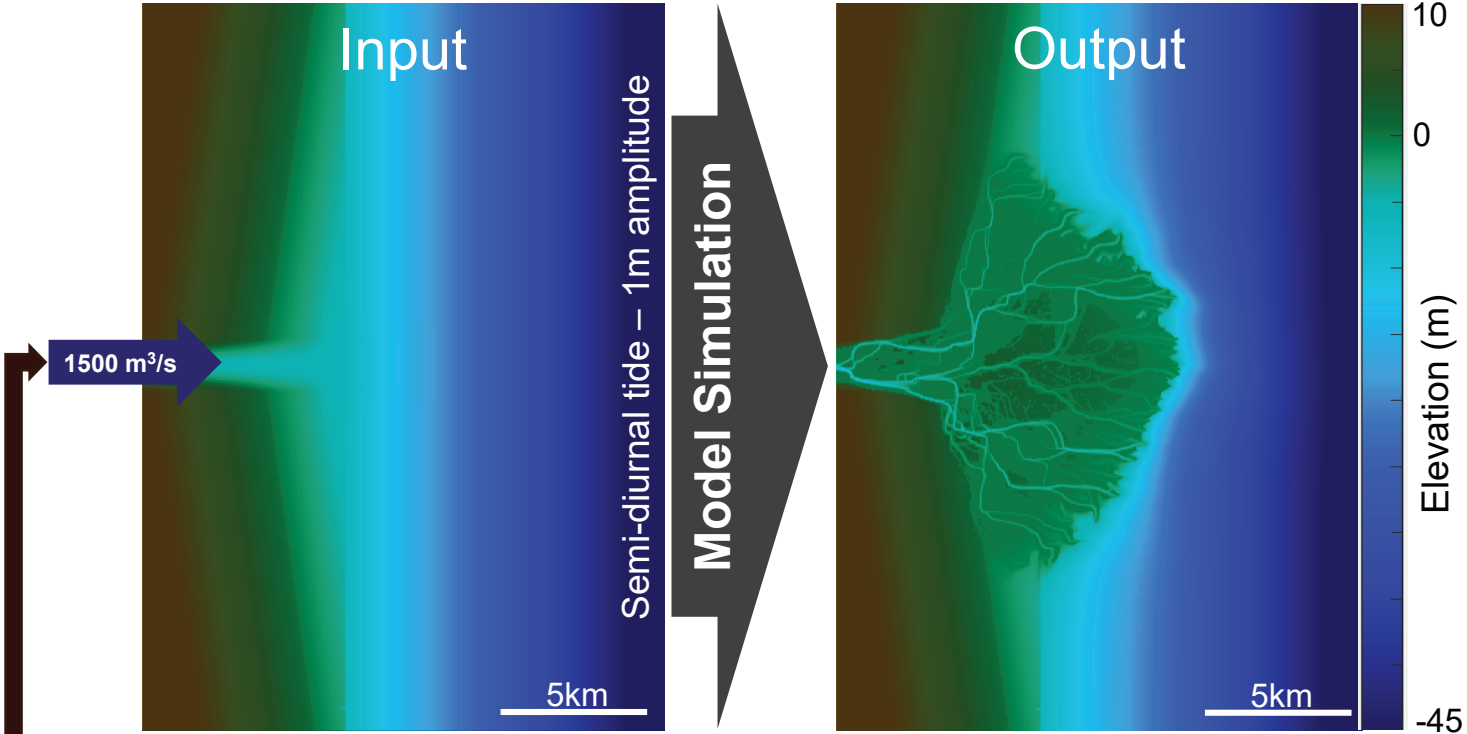
802 Fig. 11. The change in delta front slope over time for all simulations

803 Fig. 12. Averaged topography of time steps 50, 75 and 100 show apparent
804 retrogradation driven by the evolution of the central lobes of the delta (respectively A,
805 B, C) while the lateral lobes have not yet evolved. By time step 125 at least one lateral
806 lobe has started evolving after a major avulsion event, causing the averaged
807 topographical profile to level out and exhibit a progradation pattern.

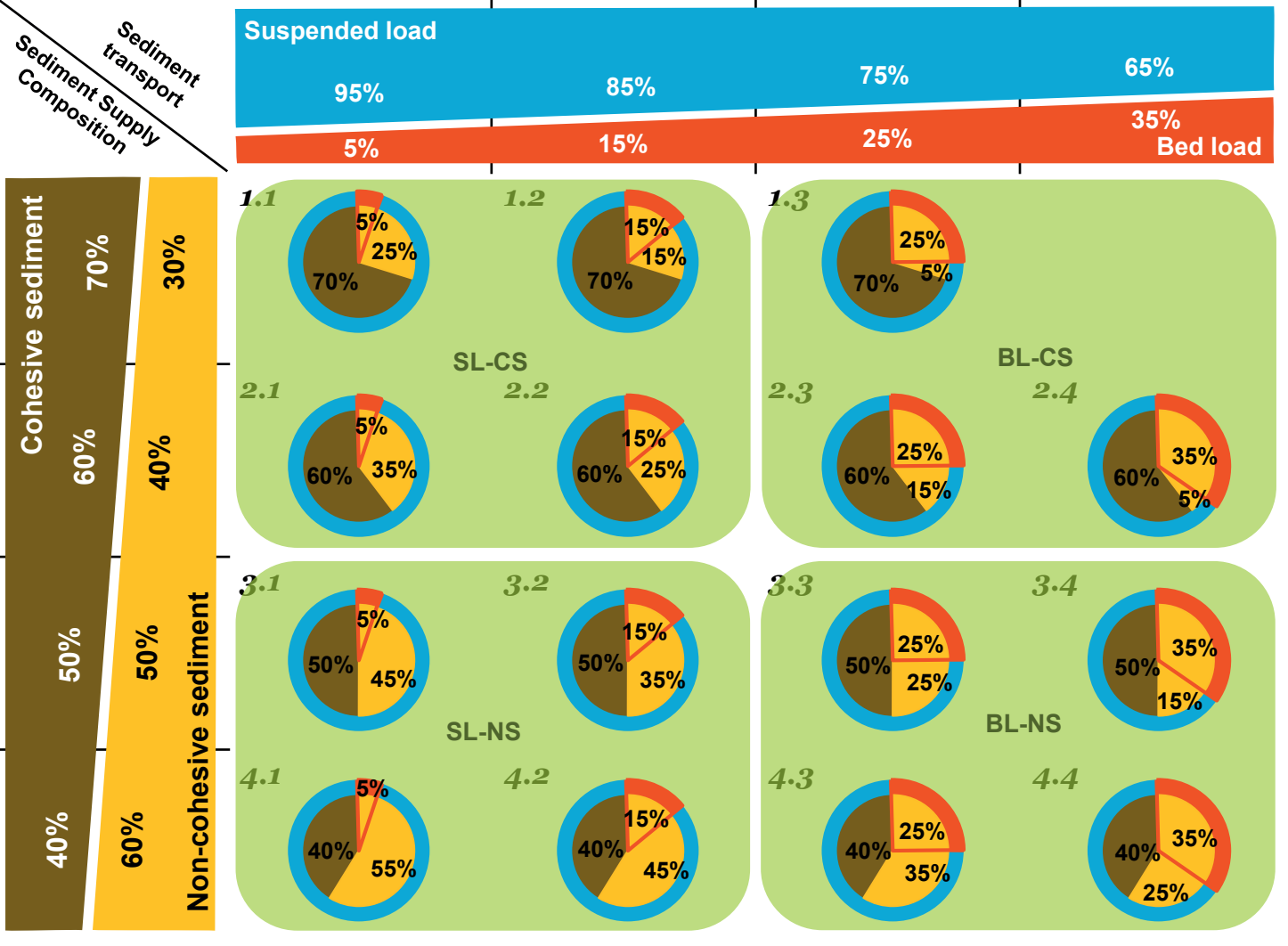
808 **Table titles**

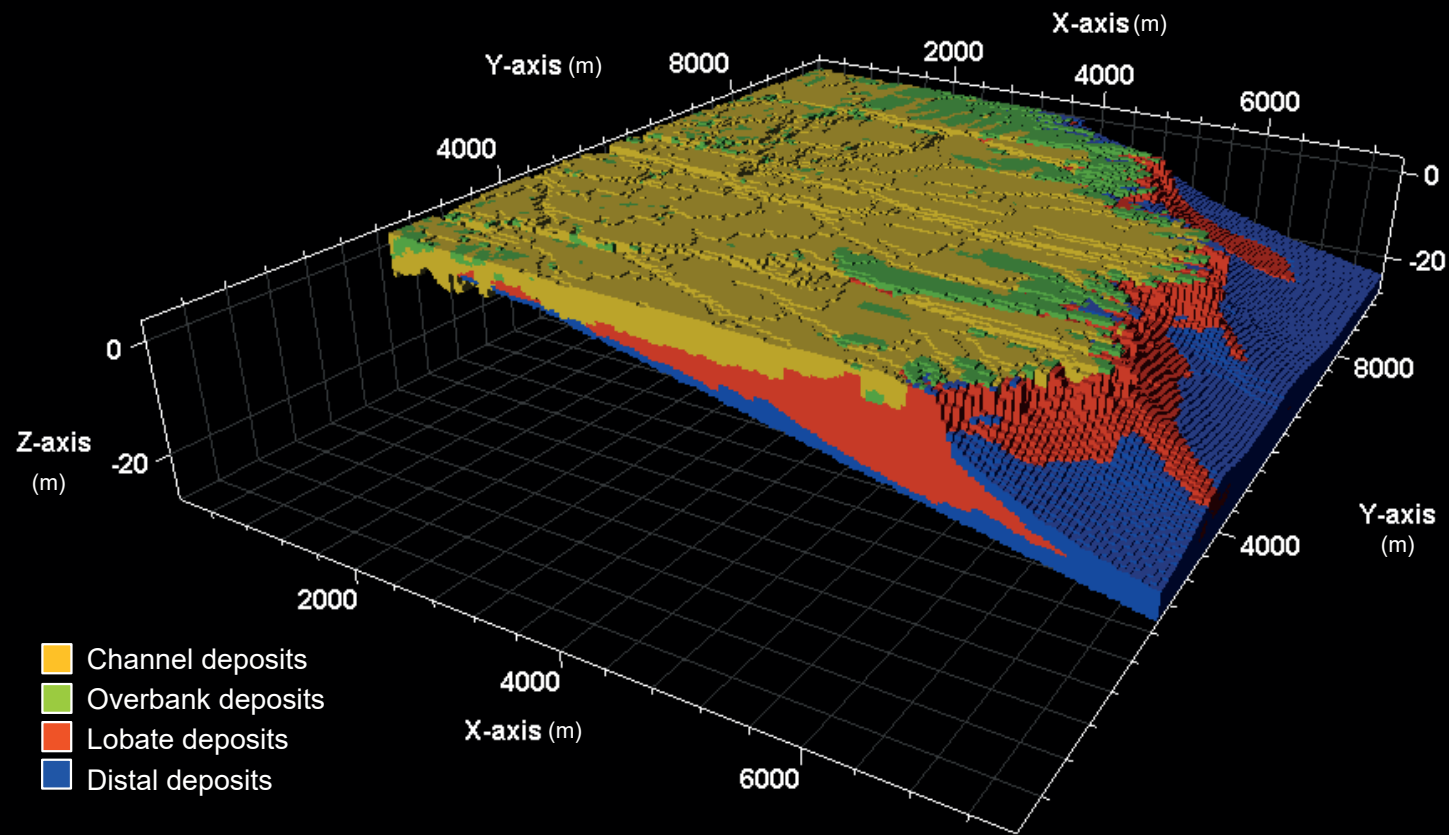
809 Table 1. Input sediment concentrations for all models as well as the resulting D_{50}
810 values.

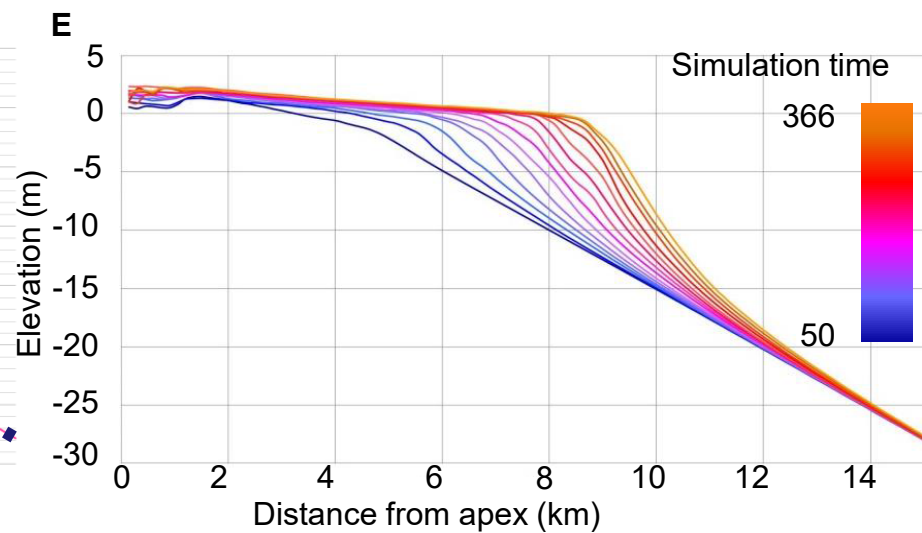
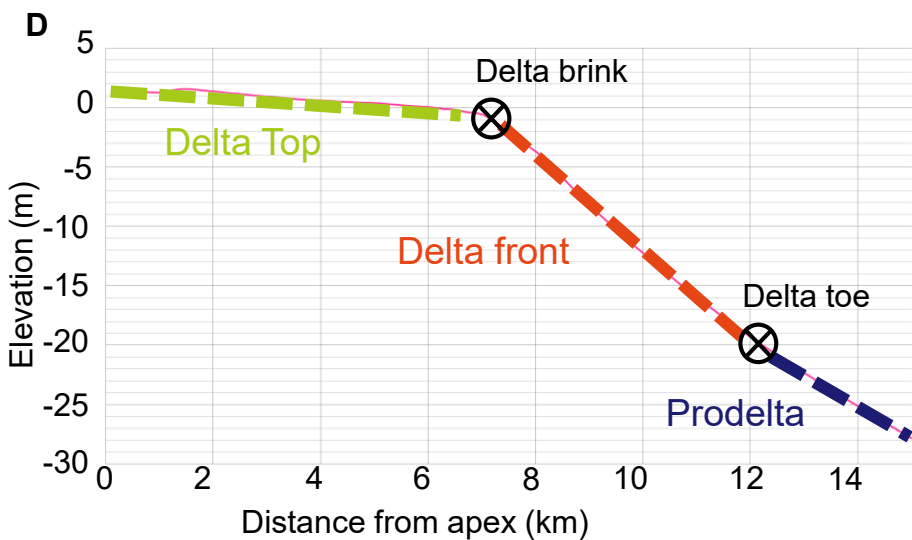
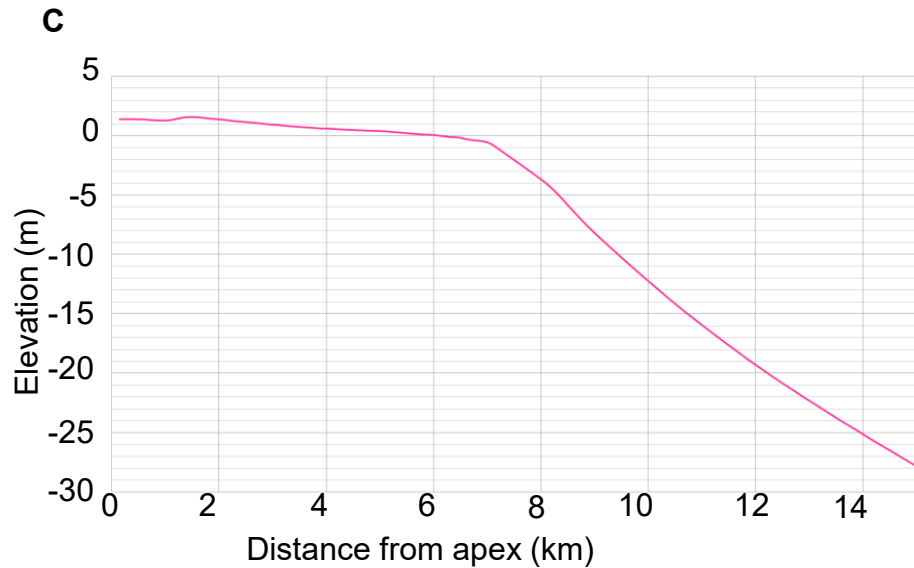
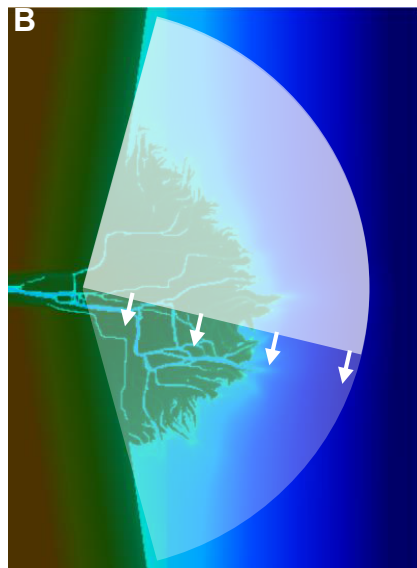
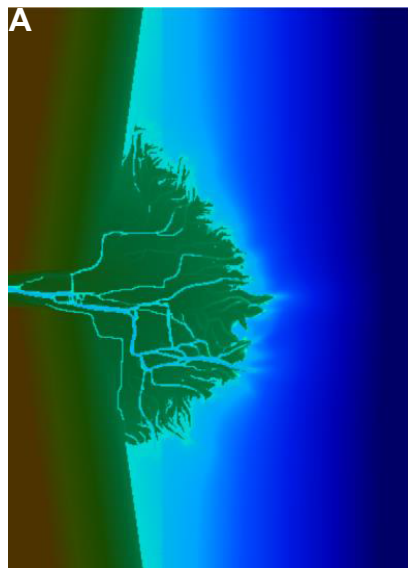
811 Table 2. Values for cumulative vertical aggradation at 2 km from the delta apex and
812 cumulative horizontal displacement for the delta brink and delta toe.

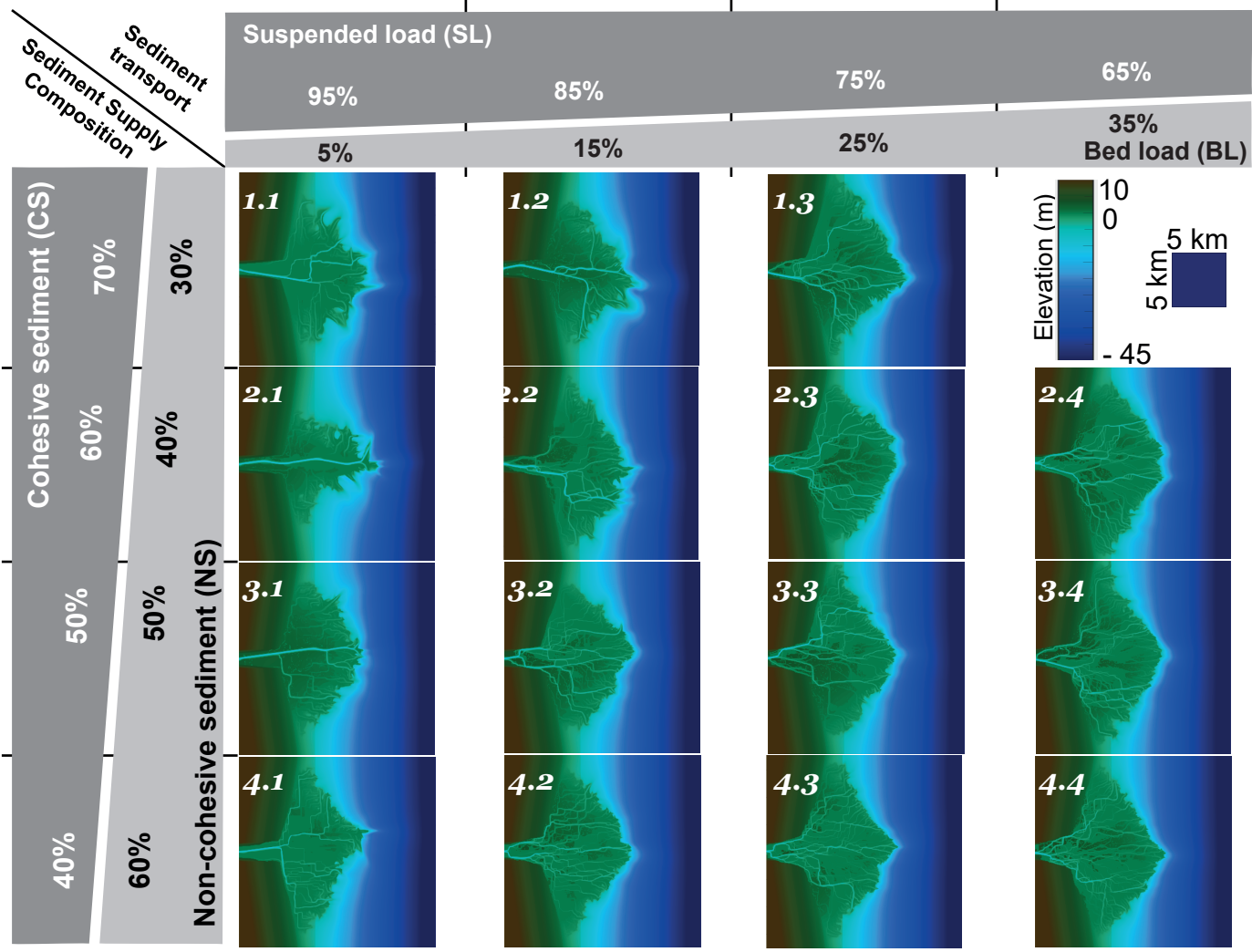


Sediment Class	Median grain size (μm)	Settling Velocity (mm/s)	Critical bed shear stress for sedimentation (N/m^2)	Critical bed shear stress for erosion (N/m^2)	Reference density for hindered settling (kg/m^3)	Specific density (kg/m^3)	Dry bed density (kg/m^3)
Non-Cohesive1	200	-	-	-	1600	2650	1600
Non-Cohesive2	100	-	-	-	1600	2650	1600
Cohesive1	-	0.86	1000	0.3	1600	2650	500
Cohesive2	-	0.25	1000	0.5	1600	2650	500







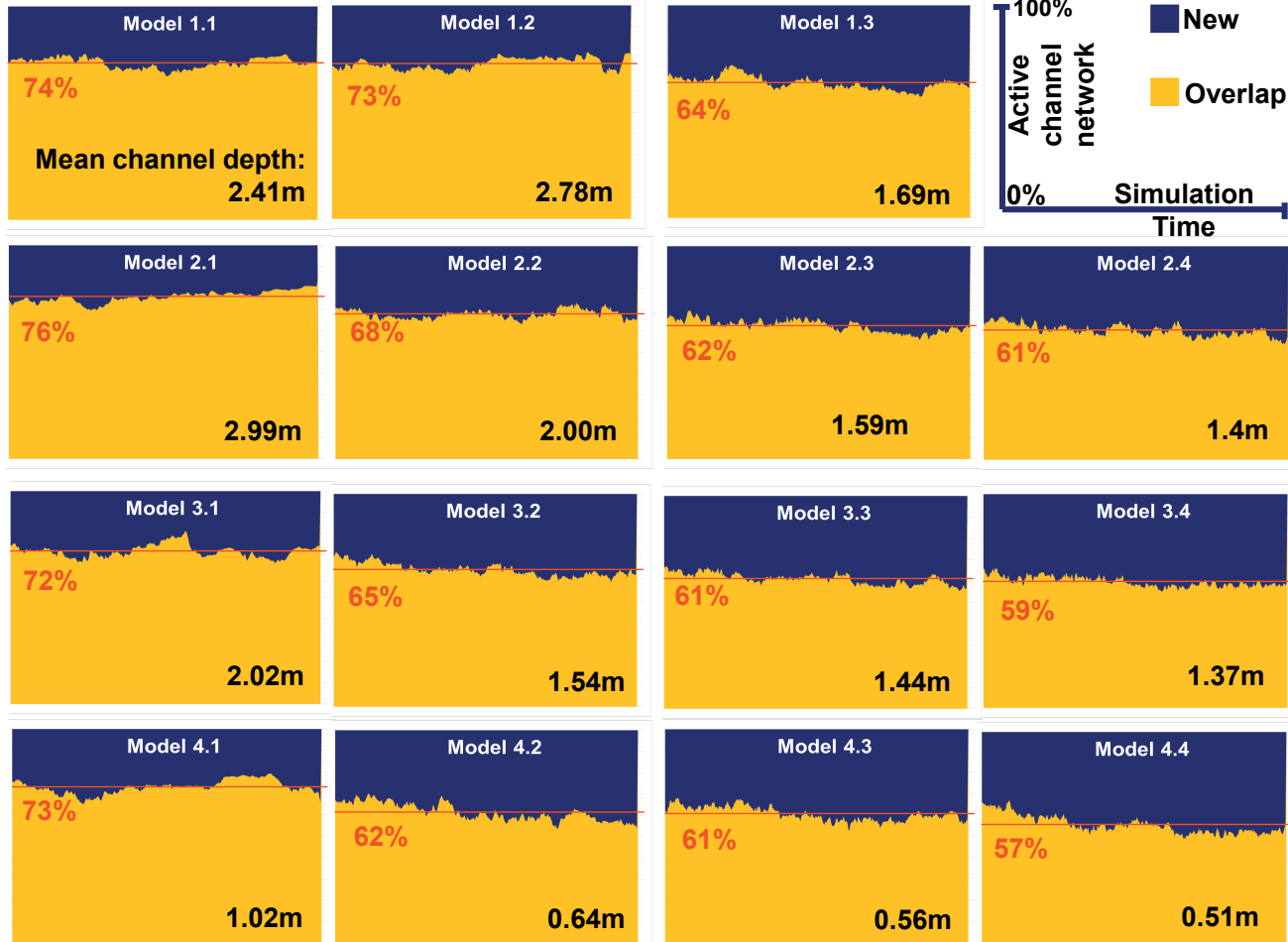


Suspended load (SL)

Bed load (BL)

Cohesive sediment (CS)

Non-cohesive sediment (NS)



Cohesive sediment (CS)

Non-cohesive sediment (NS)

Non-cohesive sediment (NS)

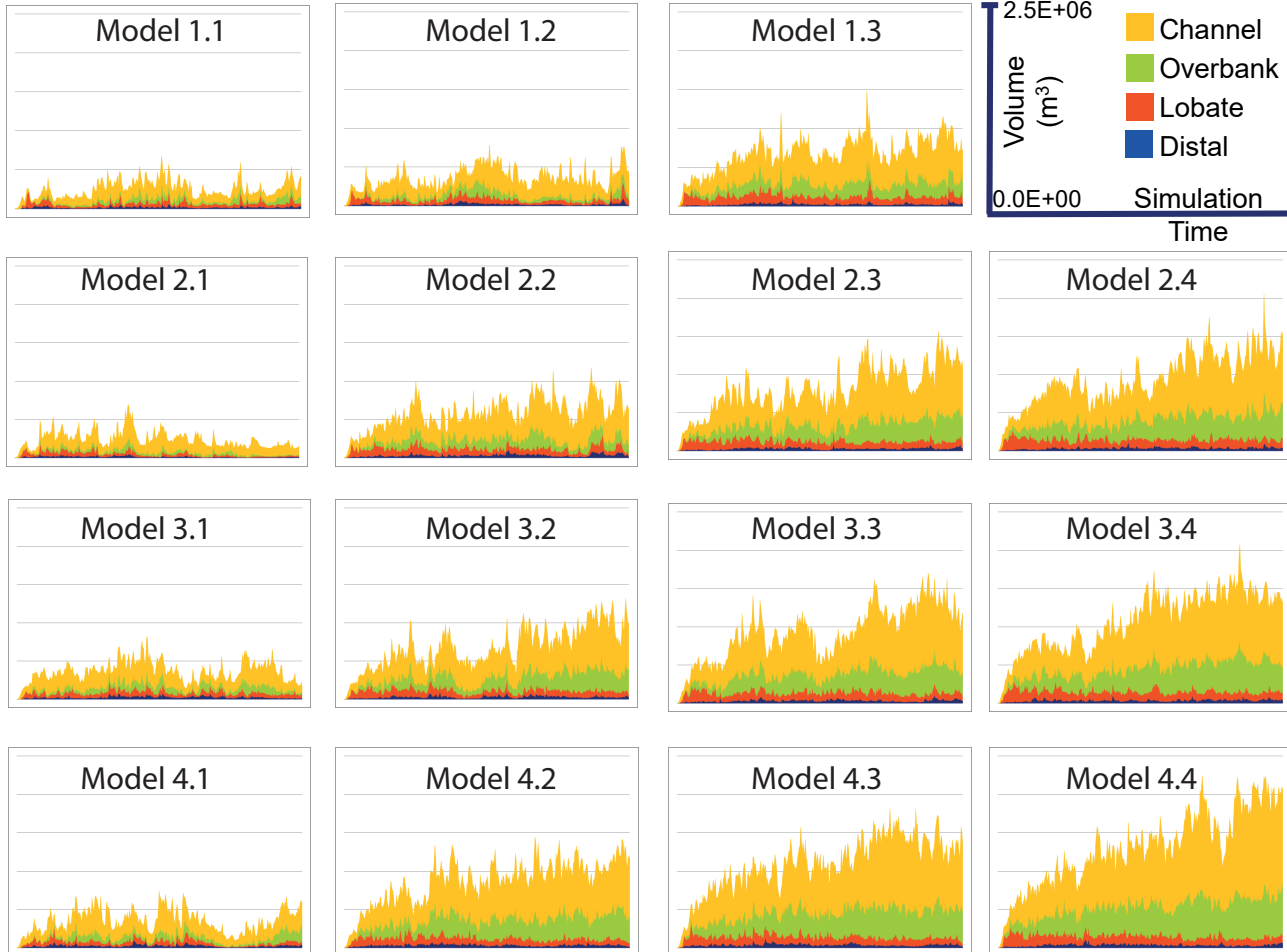


Suspended load (SL)

Bed load (BL)

Cohesive sediment (CS)

Non-cohesive sediment (NS)

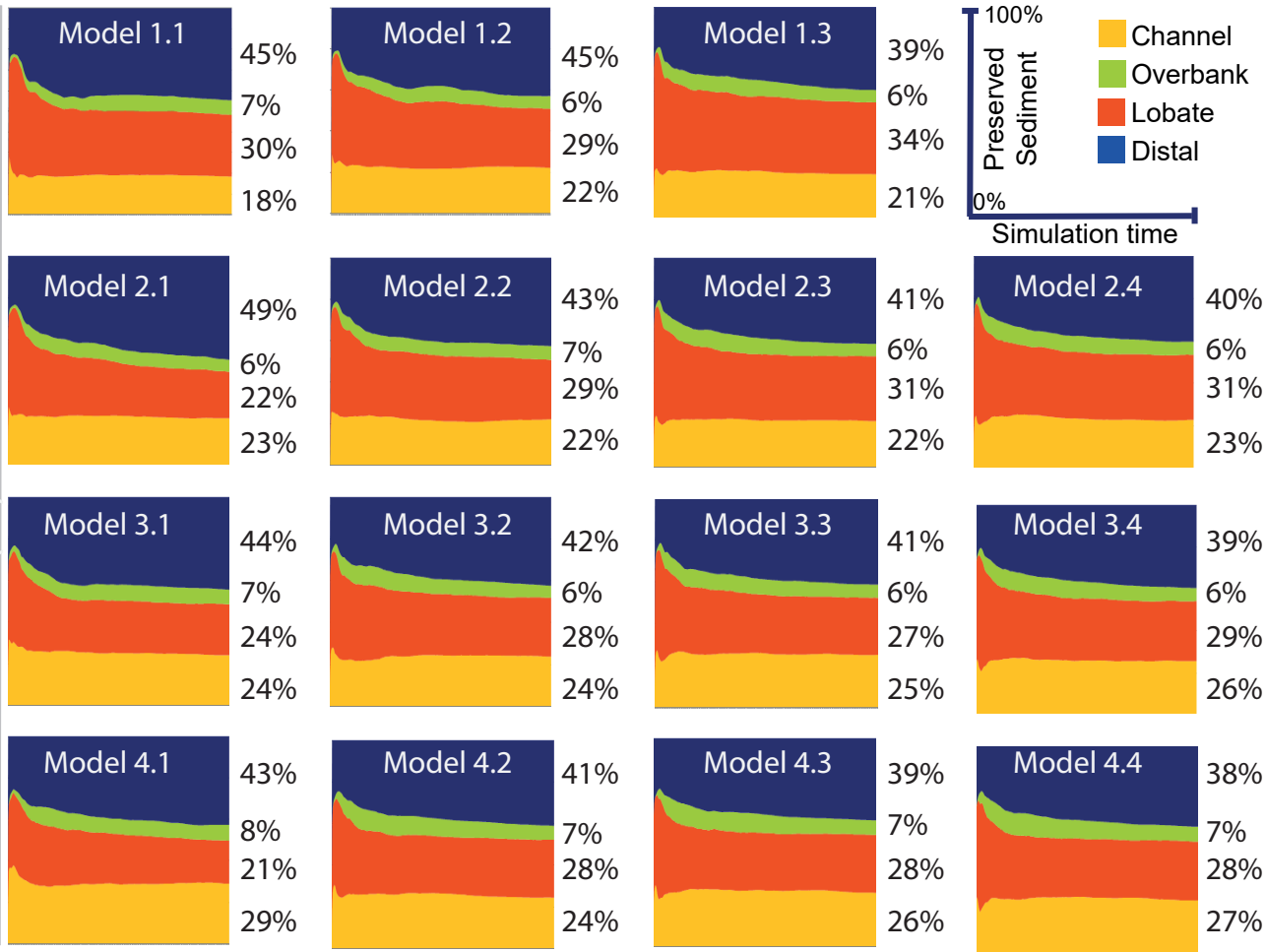


Suspended load (SL)

Bed load (BL)

Cohesive sediment (CS)

Non-cohesive sediment (NS)



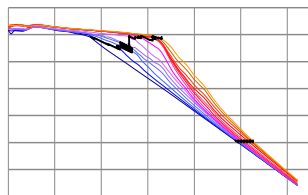
Suspended load (SL)

Bed load (BL)

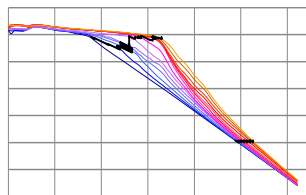
Cohesive sediment (CS)

Non-cohesive sediment (NS)

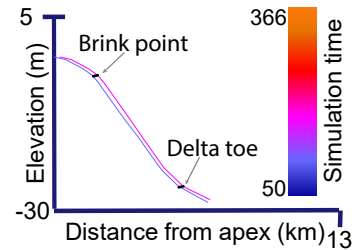
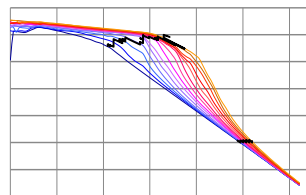
Model 1.1



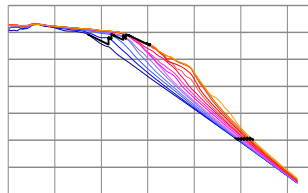
Model 1.2



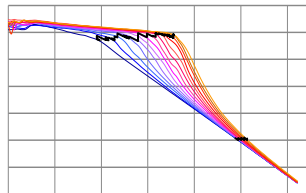
Model 1.3



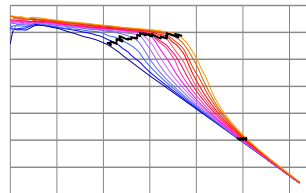
Model 2.1



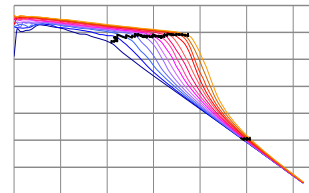
Model 2.2



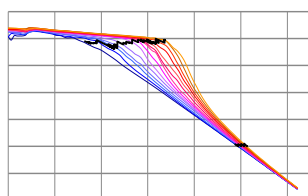
Model 2.3



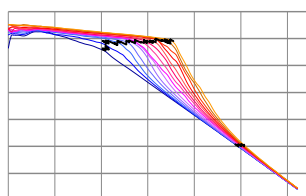
Model 2.4



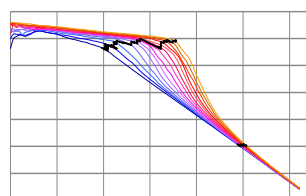
Model 3.1



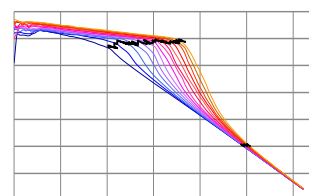
Model 3.2



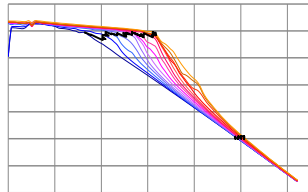
Model 3.3



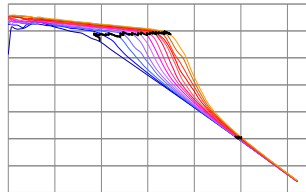
Model 3.4



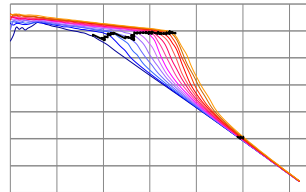
Model 4.1



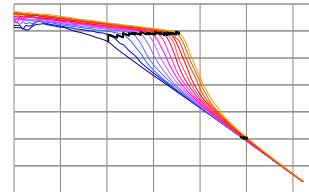
Model 4.2

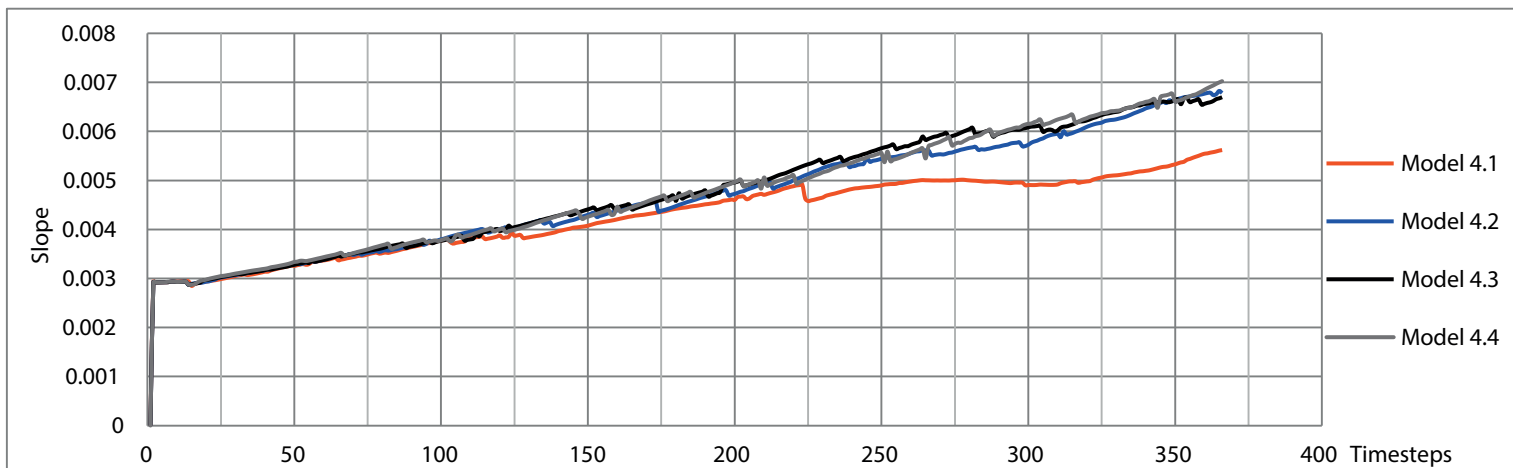
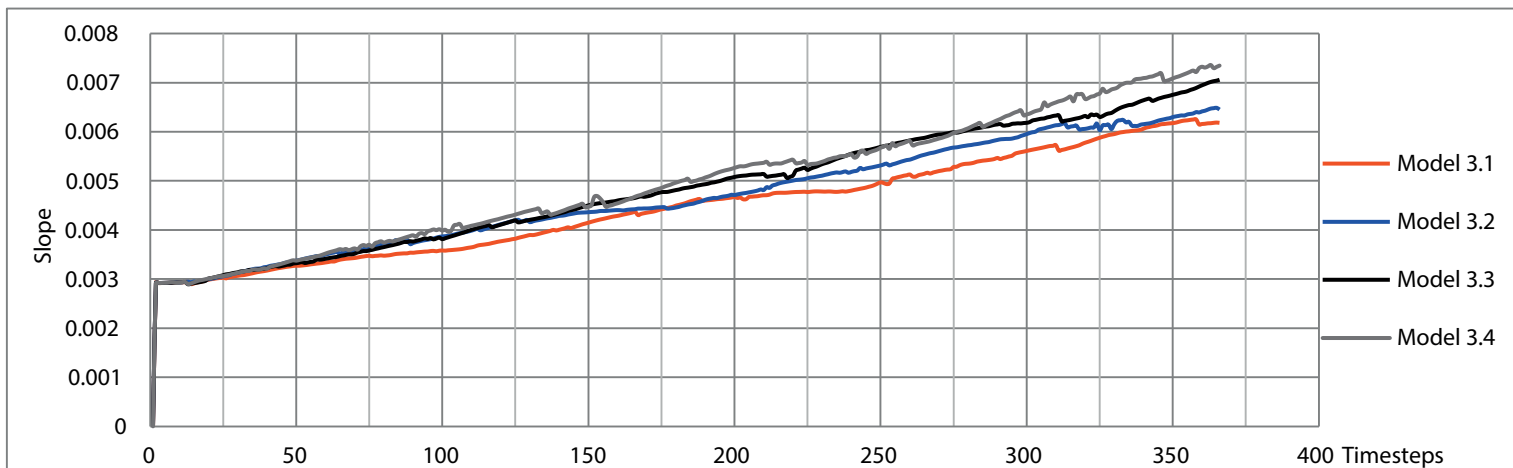
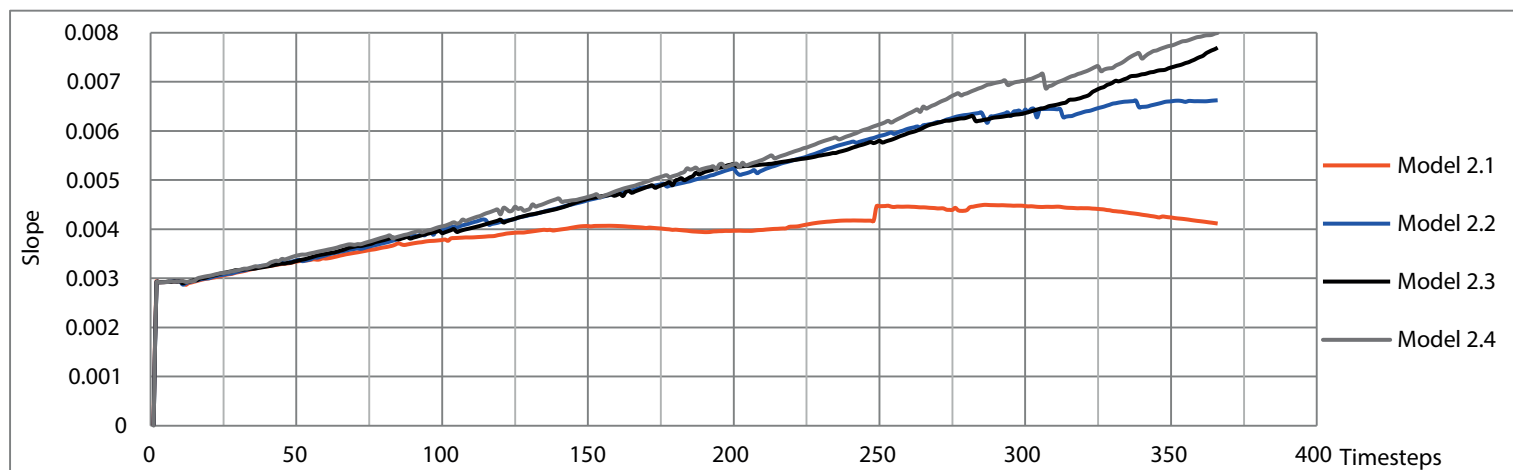
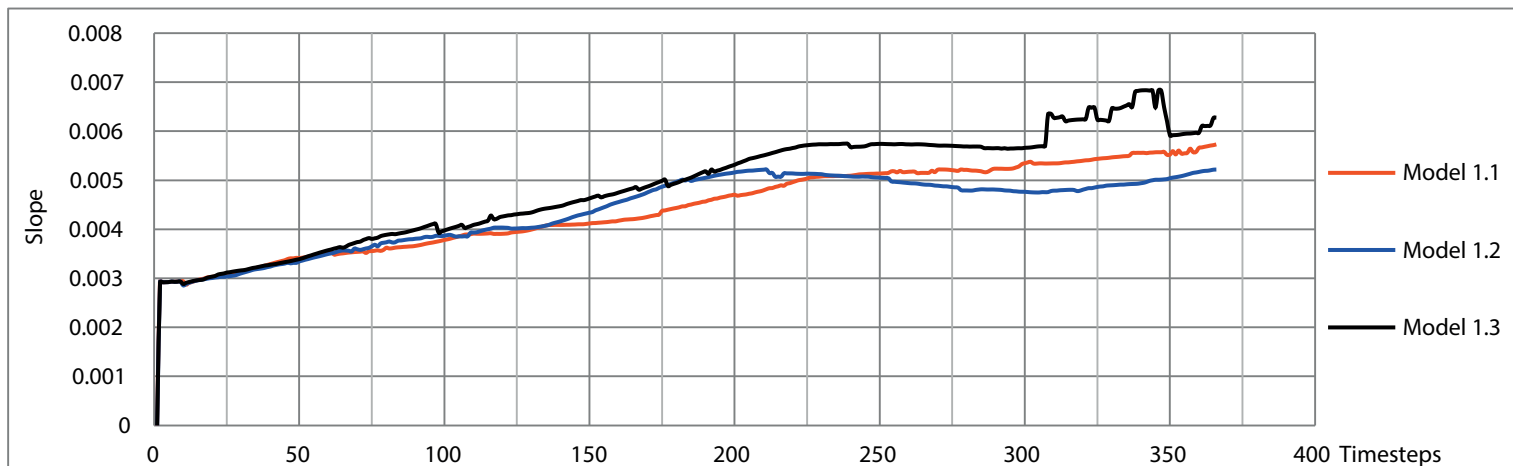


Model 4.3

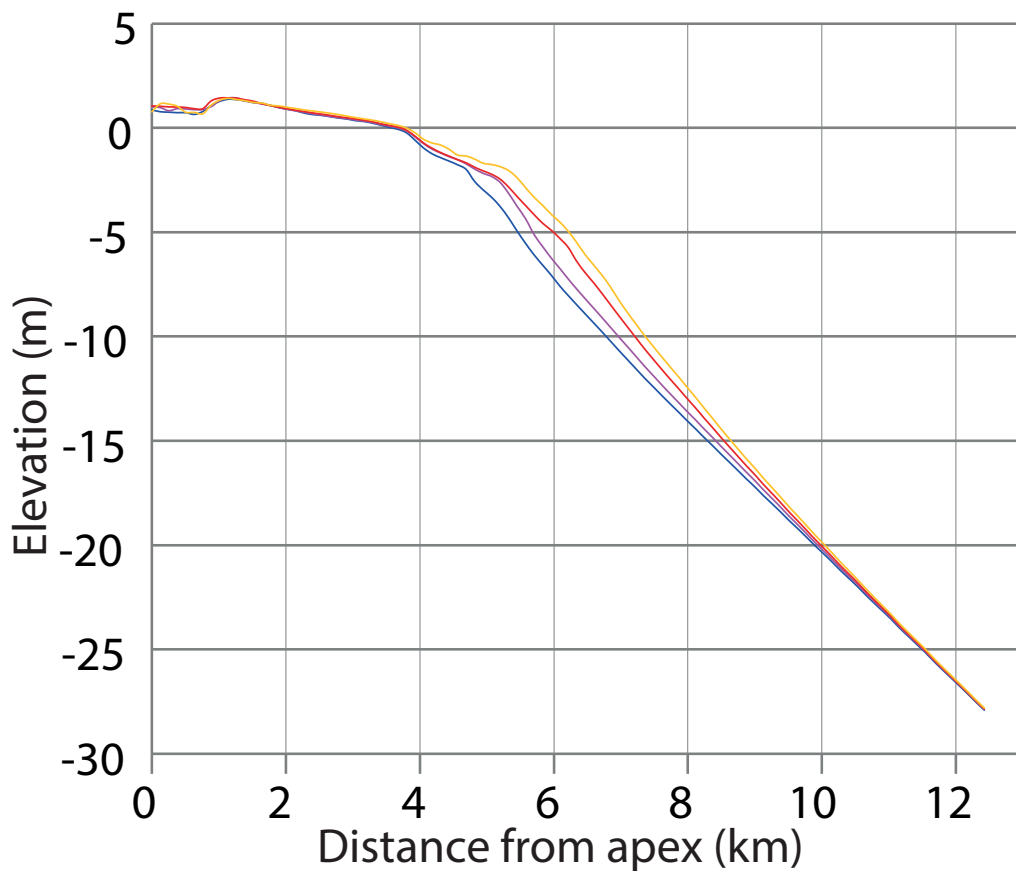


Model 4.4



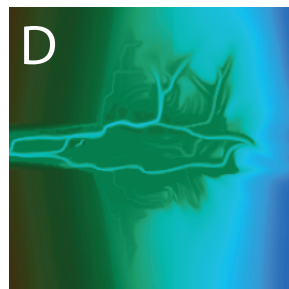
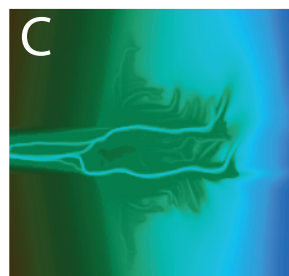
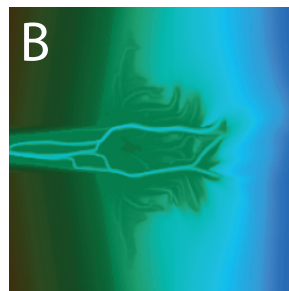
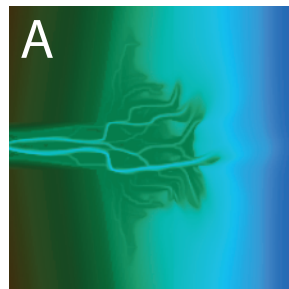
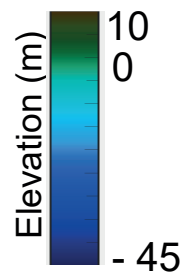
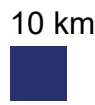


Model 1.1



- (A) Time step 50
- (B) Time step 75
- (C) Time step 100
- (D) Time step 125

10 km



	Non- Cohesive 1 (kg m ⁻³)	Non- Cohesive 2 (kg m ⁻³)	Cohesive 1 (kg m ⁻³)	Cohesive 2 (kg m ⁻³)	Cohesive sediment (%)	Overall bedload (%)	Overall D ₅₀ value (μm)
Model 1.1	0.018	0.042	0.098	0.042	70	5	76
Model 1.2	0.018	0.042	0.098	0.042	70	15	76
Model 1.3	0.018	0.042	0.098	0.042	70	25	76
Model 2.1	0.024	0.056	0.084	0.036	60	5	84
Model 2.2	0.024	0.056	0.084	0.036	60	15	84
Model 2.3	0.024	0.056	0.084	0.036	60	25	84
Model 2.4	0.024	0.056	0.084	0.036	60	35	84
Model 3.1	0.03	0.07	0.07	0.03	50	5	92
Model 3.2	0.03	0.07	0.07	0.03	50	15	92
Model 3.3	0.03	0.07	0.07	0.03	50	25	92
Model 3.4	0.03	0.07	0.07	0.03	50	35	92
Model 4.1	0.036	0.084	0.056	0.024	40	5	99
Model 4.2	0.036	0.084	0.056	0.024	40	15	99
Model 4.3	0.036	0.084	0.056	0.024	40	25	99
Model 4.4	0.036	0.084	0.056	0.024	40	35	99

	Vertical displacement at 2 km from the delta apex (m)	Horizontal brink point displacement (m)	Horizontal delta toe displacement (m)
Model 1.1	2.14	2535	1.74
Model 1.2	2.26	2409	2.08
Model 1.3	2.88	2789	1.74
Model 2.1	1.96	1902	2.08
Model 2.2	2.55	3042	1.39
Model 2.3	3.07	3296	1.04
Model 2.4	3.24	3423	1.04
Model 3.1	2.37	2535	1.39
Model 3.2	2.80	3042	1.04
Model 3.3	3.01	3042	1.04
Model 3.4	3.29	3296	1.04
Model 4.1	2.40	2155	1.04
Model 4.2	3.04	2916	0.69
Model 4.3	3.14	3042	0.69
Model 4.4	3.56	3042	0.69